Observation of subkelvin superconductivity in Cd_3As_2 thin films

A. V. Suslov,[1] A. B. Davydov,[2] L. N. Oveshnikov,[3,2,*] L. A. Morgun,[2,4] K. I. Kugel,[5,4] V. S. Zakhvalinskii,[6] E. A. Pilyuk,[6] A. V. Kochura,[7] A. P. Kuzmenko,[7] V. M. Pudalov,[2,4] and B. A. Aronzon[2]

[1]*National High Magnetic Field Laboratory, Tallahassee, Florida 32310, USA*
[2]*P. N. Lebedev Physical Institute, Russian Academy of Sciences, Moscow 119991, Russia*
[3]*National Research Center "Kurchatov Institute," Moscow 123182, Russia*
[4]*National Research University Higher School of Economics, Moscow 101000, Russia*
[5]*Institute for Theoretical and Applied Electrodynamics, Russian Academy of Sciences, Moscow 125412, Russia*
[6]*Belgorod National Research University, Belgorod 308015, Russia*
[7]*South-West State University, Kursk 305040, Russia*

(Received 14 November 2018; published 14 March 2019)

We report an experimental observation of superconductivity in Cd_3As_2 thin films without application of external pressure. The films under study were synthesized by magnetron sputtering. Surface studies suggest that the observed transport characteristics are related to the polycrystalline continuous part of the investigated films with a homogeneous distribution of elements and the Cd-to-As ratio close to stoichiometric Cd_3As_2. The latter is also supported by Raman spectra of the studied films where two pronounced peaks inherent to Cd_3As_2 were observed. The obtained x-ray diffraction patterns for studied films also correspond to the Cd_3As_2 lattice. The formation of a superconducting phase in the films under study is confirmed by the characteristic behavior of the temperature and the magnetic field dependence of the sample resistivity, as well as by the presence of pronounced zero-resistance plateaus in the dV/dI characteristics. The corresponding H_c-T_c plots reveal a clearly pronounced linear behavior within the intermediate temperature range, similar to that observed for bulk Cd_3As_2 and Bi_2Se_3 films under pressure, suggesting the possibility of a nontrivial pairing in the films under investigation. We discuss a possible role of the sample inhomogeneities and crystal strains in the observed phenomena.

DOI: 10.1103/PhysRevB.99.094512

I. INTRODUCTION

Weyl and Dirac semimetals (WSM and DSM) currently attract wide interest related to the existence of Dirac nodes in their electron spectrum and related nontrivial topological characteristics of both bulk and surface states [1–3]. Special attention is drawn to the Cd_3As_2 compound, which proved to be air stable, unlike some other DSM materials [4–8]. This compound is known and has been studied for quite a long time [9–12]. Nevertheless, it is still very popular since the Dirac nodes of this semimetal are protected by the crystal symmetry and the electron states exhibit interesting topological properties, such as spin-momentum locking. Due to the high symmetry, DSM materials can undergo transitions to other topological phases (e.g., WSM) as a result of breaking certain symmetries or applying some external factors.

The existence of topologically protected electron states gives a new impetus to the problem of topological superconductivity (TSC) that has been discussed for a long time [13–15]. In particular, Sato *et al.* [16,17] performed a theoretical analysis of the possible types of superconducting (SC) pairing in Cd_3As_2-type systems, including topologically nontrivial ones. Basically, the existence of a nontrivial pairing potential (leading to the emergence of triplet Cooper pairs) should induce the formation of Majorana modes at the surface of the crystal, which can be used in fault-tolerant quantum computing [14]. The emergence of a SC phase in Cd_3As_2 was reported for bulk crystals [18], however, it was observed at pressures above the structural transition from the tetragonal to trigonal phase. While theoretical works suggest the stabilization of the TSC phase upon such symmetry lowering [16,17], such a transition also implies the appearance of a gap at the Dirac nodes, thus suppressing the DSM phase. Additional indications of the SC phase in Cd_3As_2 were also observed in point-contact spectroscopy experiments and attributed to local crystal distortions under the point contact [19,20]. It is important to note that, up to now, all indications of the emergence of a SC phase in Cd_3As_2 were related either to pressure-induced structural changes or to the proximity effect with conventional *s*-wave SC [21–23].

Recent studies of Cd_3As_2 thin films outlined their specific features. The observation of a quantum Hall state [24,25] and a consecutive analysis of magnetoresistance of Cd_3As_2 films suggest the occurrence of Weyl orbits related to the surface states below some critical thickness [26,27]. Thus, a superconducting Cd_3As_2 thin film with nontrivial pairing (TSC state) should yield surface Majorana modes, which, however, can be modified (in comparison to the bulk crystal [16]) due to the interaction of opposite surfaces.

In previous studies, bulk Cd_3As_2 has not exhibited any indications of superconductivity except that arising at extremely high pressures. In contrast to this, we have observed superconductivity in Cd_3As_2 thin films without external compression.

*oveshln@gmail.com

We argue that the observed phenomena cannot be related to any parasitic effects and they have certain similarities to the previously observed SC in Cd_3As_2 under pressure [18], suggesting the possible presence of nontrivial pairing in the studied films.

II. METHODS

The films under study were deposited by high-frequency magnetron nonreactive sputtering, performed with a nominal radiation power of 10 W in Ar atmosphere with a residual pressure of 0.7 Pa. Single crystals of Cd_3As_2 used for sputtering were grown by vapor phase deposition from high-purity initial components. In this paper, we present the results for three films, shaped into a Hall bar geometry with a mm-scale conduction channel. Samples A and C were deposited onto polished p-Si substrates ($\rho_{sub} = 2\ \Omega\,cm$) with a native oxide layer, and sample B was deposited onto an Al_2O_3 substrate. During the deposition, the substrates were kept at room temperature. The deposition time for samples A and C was 20 min, and for sample B it was 40 min.

The initial surface studies of the grown films were conducted using the scanning electron microscope (SEM) JSM-6610LV (JEOL, Japan) with an additional X-Max^N module (Oxford Instruments, U.K.) for energy-dispersive x-ray spectroscopy (EDXS). For imaging, we used detectors for secondary and backscattered electrons. Additional studies were performed using the atomic-force microscope (AFM) SmartSPM 1000 (AIST NT, USA). Raman spectra were recorded at room temperature using a combined scanning probe microscopy system with a confocal fluorescence spectrometer and the Raman spectrometer OmegaScope^{TM} (AIST NT, USA). For excitation we used a laser with a 532-nm wavelength, power of 50 mW, and a focused light spot at the sample surface of about 500 nm. The spectral resolution was 0.8 cm^{-1}.

The x-ray diffraction (XRD) patterns of the studied samples were obtained using the GBC EMMA analyzer (GBC Scientific Equipment, Australia) with a Cu radiation source ($\lambda = 1.541\,84$ Å). Due to the sample geometry, the obtained XRD data also contain pronounced peaks related to the aluminum sample holder.

To eliminate all uncertainties related to the experimental artifacts in the measurements of the transport properties of the samples, we used two different setups. Samples A and B were studied using a cryogen-free dilution refrigerator BF-LD250 with a 1-T magnet (BlueFors, Finland) at the Lebedev Shared Facility Center, Moscow, Russian Federation. Those experiments were performed by a conventional low-frequency (7.142 Hz) lock-in four-probe method with measurement currents (of the order of 100 nA) considerably lower than the critical values obtained for the studied films. Sample C was studied using a 20-T superconducting magnet with a dilution refrigerator (SCM1) at the National High Magnetic Field Laboratory (NHMFL), Tallahassee, Florida, USA. There, a Model No. 372 ac resistance bridge with a preamp 3708 (Lake Shore Cryotronics, Inc., USA) was used for magnetoresistance testing by the four-probe method at a current of 316 nA. Measurements of the differential resistance dV/dI were performed utilizing a current source Model No. 6221 and a nanovoltmeter Model No. 2182A (Tektronix, Inc., USA).

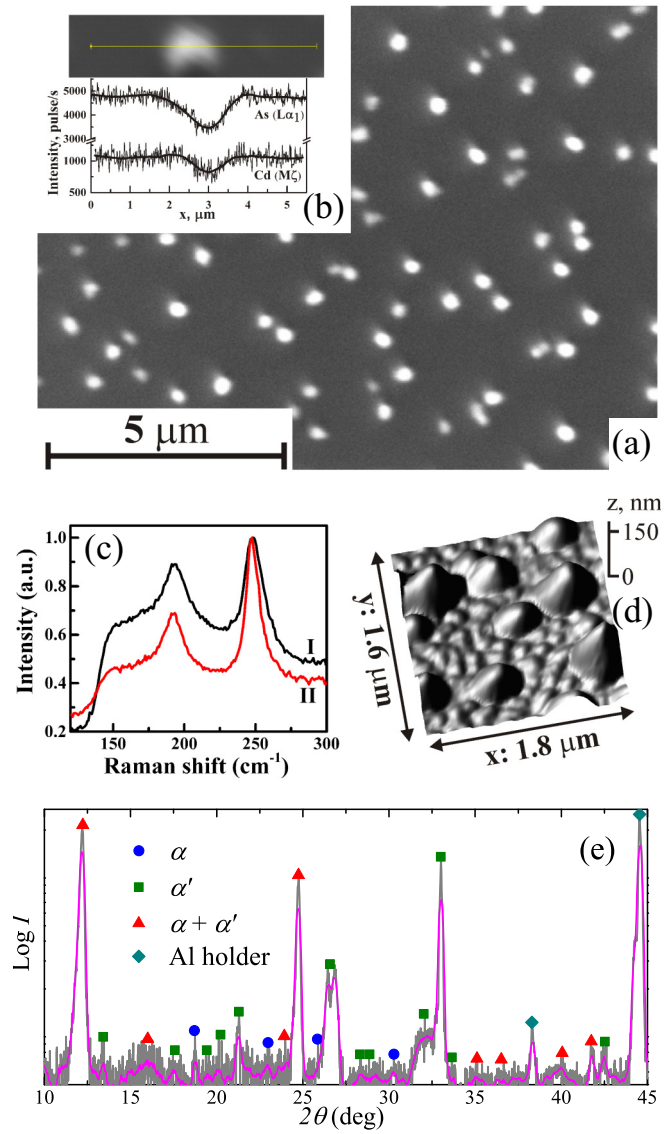

FIG. 1. (a) SEM image of the sample C surface. Light regions correspond to large grains at the surface of continuous films. (b) EDX scan: Distribution of the Cd- and As-related peak amplitudes within a one-dimensional (1D) scan across a surface grain as illustrated above. The corresponding amplitudes decrease in the surface grain area due to the "shadowing" effect related to the 3D shape of a surface grain. The Cd-to-As ratio within the whole scanning area is close to stoichiometric Cd_3As_2. (c) Raman spectra for sample C (I) and reference Cd_3As_2 single crystal (II). (d) 3D visualization of the AFM image of the surface of sample C. (e) XRD pattern for sample A (magenta line, smoothed data). The obtained pattern corresponds to α and α' modifications of the Cd_3As_2 lattice (see text).

III. EXPERIMENTAL RESULTS

SEM images of the studied films reveal a similar surface morphology. As one can see in Fig. 1(a), there are large grains at the surface of the continuous film. The presence of such hemispherical grains corresponds to the island-type growth process of the film, which is quite common for various

methods of physical deposition. These grains have typical sizes of about 100–300 nm, while the distances between them are substantially larger. The latter suggests the absence of such grain overlapping, implying that the transport properties are determined by the continuous part of the film located beneath them. The EDX mapping reveals a homogeneous distribution of components [Fig. 1(b)], implying that the transport characteristics of the film are related solely to the Cd-As binary system. The EDXS demonstrates that at μm scale the Cd-to-As ratio is constant and close to the stoichiometric Cd_3As_2 within 2% accuracy (according to a quantitative analysis of the EDX spectra, not provided in this paper). The presence of the Cd_3As_2 phase is also supported by the Raman spectroscopy results. A typical Raman spectrum for the studied films is shown in Fig. 1(c) (curve I). As a reference, we also provide the Raman spectrum for the Cd_3As_2 single crystal used as a target for sputtering (curve II). Earlier, it was shown that the presence of two main peaks around 200 and 250 cm^{-1} is a characteristic feature of the Raman spectra for Cd_3As_2 nanocrystallites [28] and thin films [29] measured at room temperature using unpolarized light. The obtained AFM images show that the surface regions between large grains are formed by smaller (about 40–50 nm) overlapping grains [Fig. 1(d)], suggesting the polycrystalline structure of the continuous part of the film. The thickness of the studied films determined by AFM is 40–50 nm for samples A and C, and about 80 nm for sample B.

While almost all theoretical considerations of Cd_3As_2 refer solely to single crystals, there are no profound arguments that the DSM phase will be inevitably absent in a polycrystalline sample, since the main features of the band structures in solids are usually formed at the scale of several lattice constants. Obviously, when the crystallite size is reduced down to the nm scale, the quantum size effect can substantially alter the band structure. Although there is no accurate estimation of the nanocrystallite critical size, below which the DSM phase vanishes, typical Cd_3As_2 polycrystals are commonly used for the search for nontrivial topological features (e.g., the realization of the TSC state [20]).

The structure of the studied films was also investigated using XRD. The corresponding XRD pattern for sample A is shown in Fig. 1(e). Except for two peaks related to the sample holder, the obtained patterns, including low-intensity peaks, can be interpreted in terms of α (space group $I4_1/acd$, $a = 12.6461$ Å, $b = 25.4378$ Å) and α' (space group $P4_2/nbc$, $a = 12.6848$ Å, $b = 25.4887$ Å) modifications of the Cd_3As_2 lattice [30]. The main difficulty is that both α and α' modifications have tetragonal lattices with very close unit cell parameters. Thus, the corresponding diffraction peaks are very close to each other, and several of them are simply indistinguishable [marked as $\alpha + \alpha'$ in Fig. 1(e)]. While the appearance of the α'-Cd_3As_2 phase in our case can be related to the fast cooling of the film during the synthesis process [31], the existence of two polymorphic phases agrees well with the polycrystalline structure of the studied films. A very subtle difference between the α and α' lattices suggests that the corresponding electron spectra are also very close, implying the existence of the DSM phase in both cases. We should also mention that the most intense diffraction peak at $2\theta \approx 12^\circ$ corresponds to the (112) plane and suggests a

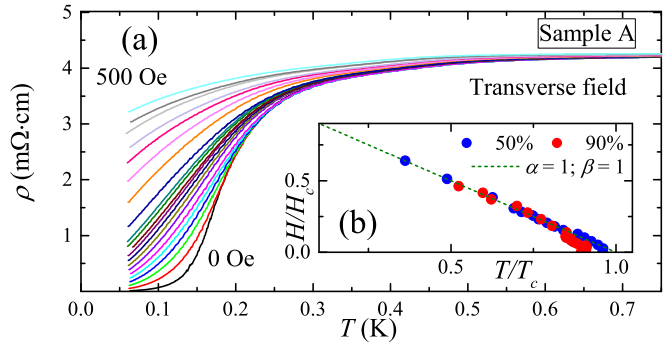

FIG. 2. (a) Temperature dependence of resistivity for sample A at various transverse magnetic fields. (b) Corresponding H_c-T_c diagrams for the SC transition estimated as a resistance drop to 50% (midpoint) and 90% of the normal value. Fitting of experimental data by Eq. (1) is shown by the dashed line.

partial orientation of crystallites in the film. The width of this peak corresponds to the mean crystallite size of about 35 nm (estimated using the standard Debye-Scherrer equation with a shape factor of 0.9), which agrees well with the sizes of grains in the continuous part of the film determined by AFM [see Fig. 1(d)].

Transport measurements of the studied films reveal a clearly pronounced SC transition below 0.5 K. In Fig. 2(a), we show the temperature dependence of resistivity for sample A at various values of the transverse magnetic field. As one can see, there is a distinct resistance drop (to almost zero value, of the order of the measurement noise level) that shifts to the lower temperatures upon increasing magnetic field, which supports the assumption of the emergence of the SC phase. Sample B demonstrates an analogous behavior [see Fig. 3(a)]. The actual transition regions are rather broad, which agrees well with the polycrystalline structure of the films.

The dV/dI characteristics (not to be confused with the tunnel spectra) for sample C measured at various temperatures clearly demonstrate zero-resistance plateaus [Fig. 4(a)]. The critical current values I_c decrease as the temperature approaches T_c [Fig. 4(b)]. However, at the lowest temperatures I_c appears to be temperature independent. The magnetoresistivity (MR) of sample C exhibits typical features of a field-induced SC-to-normal state transition [Figs. 5(a) and 5(b)]. As

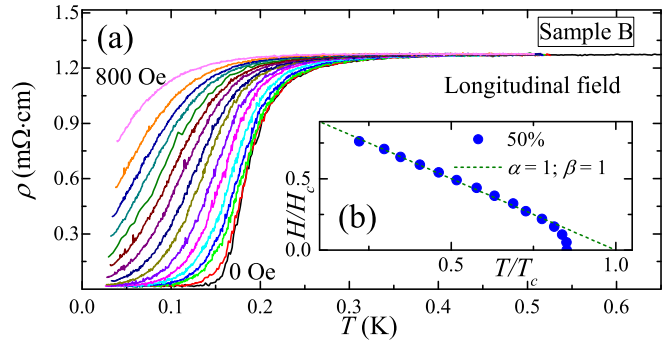

FIG. 3. (a) Temperature dependence of resistivity for sample B at various longitudinal magnetic fields. (b) Corresponding H_c-T_c diagrams for the SC transition (midpoint). Fitting of experimental data by Eq. (1) is shown by the dashed line.

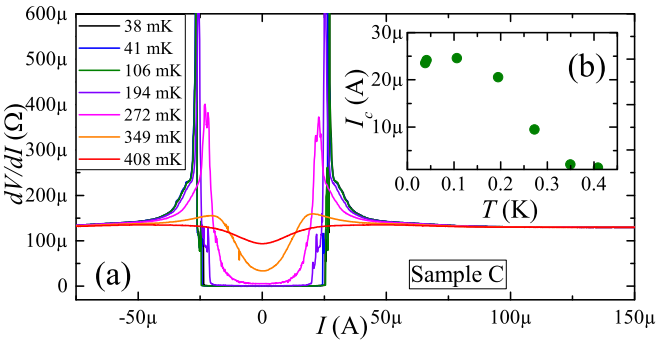

FIG. 4. (a) Differential resistance for sample C at various temperatures. (b) Corresponding temperature dependence of critical current I_c.

the temperature increases, the zero-field resistivity becomes higher, although the shape of the MR curves remains similar. We clearly observe anisotropy of the critical magnetic field: H_c values for the longitudinal field are considerably higher than those for the transverse field, which is common for thin SC films.

Assuming that H_c corresponds to the 50% resistance drop of its normal value (midpoint), we obtained H_c-T_c diagrams

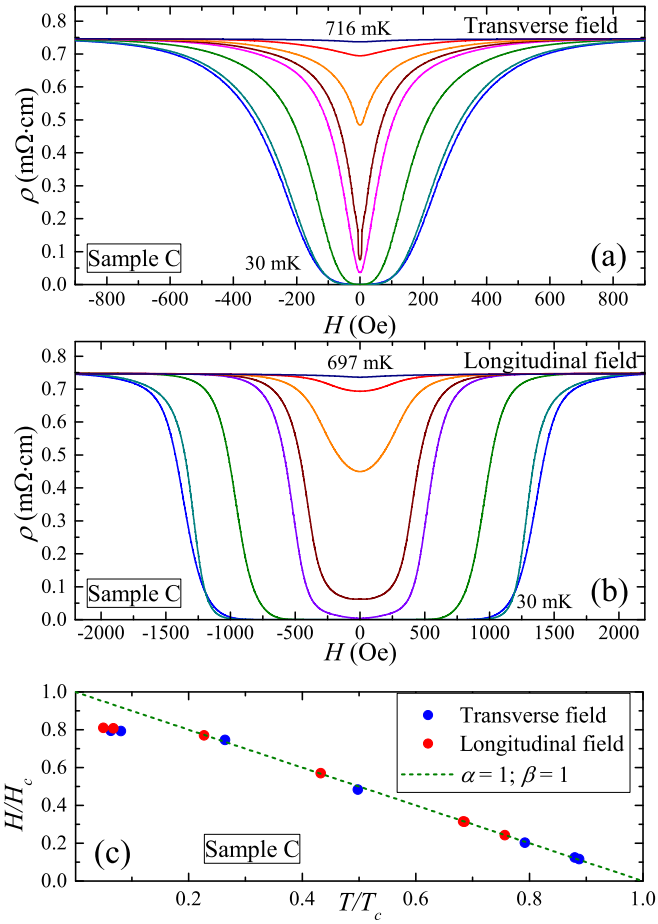

FIG. 5. Low-field magnetoresistivity of sample C at various temperatures at (a) transverse and (b) longitudinal magnetic fields. (c) Corresponding H_c-T_c diagrams for the SC transition.

for the studied samples [Figs. 2(b), 3(b), and 5(c)]. To characterize the observed SC state, we applied the conventional formula describing the decrease in the critical magnetic field H_c upon increasing the temperature below the critical value T_c,

$$H(T) = H_c(0)\left[1 - \left(\frac{T}{T_c}\right)^{\alpha}\right]^{\beta}. \quad (1)$$

Here, $\alpha = 2, \beta = 1$ corresponds to the common Bardeen-Cooper-Schrieffer (BCS) theory at low temperatures, while the Ginzburg-Landau (GL) theory suggests $\alpha = 1, \beta = 1$ to describe the temperature dependence of the upper critical field H_{c2} in type-II SC close to T_c. It is important to note that the presented H_c-T_c diagrams for the studied samples cannot be approximated well by Eq. (1) with $\alpha = 2, \beta = 1$. However, in the intermediate temperature range, the obtained diagrams can be effectively described with a linear function ($\alpha = 1, \beta = 1$) as it is shown in the corresponding figures. The deviations from this line in the vicinity of T_c (samples A and B) and low-temperature saturation (sample C) require additional investigations and can be related to the polycrystallinity of the studied films. Nevertheless, the overall behavior of the H_c-T_c diagrams for transverse and longitudinal magnetic fields is essentially the same. It is worth mentioning that there is no qualitative difference if we ascribe T_c and H_c to the 90% value of the normal state resistivity [see Fig. 2(b)].

IV. DISCUSSION

The absence of elemental segregation (confirmed by EDXS results) implies that the observed SC phase cannot be attributed to the elemental Cd, which is a classical SC with $T_c = 0.56$ K and $H_c \approx 30$ Oe [32,33] (also, the H_c values for the studied films are substantially higher, e.g., for sample A, the transverse $H_c \approx 350$ Oe). Additionally, due to the relatively large sizes of the conducting channel, the observed SC cannot be related to an influence of the contact regions. Thus, we can conclude that the observed SC phase emerges within the Cd-As binary system with the elemental ratio close to the stoichiometric Cd_3As_2 compound. Alongside the observed features in the XRD patterns and Raman spectra (inherent to the Cd_3As_2 crystal phase), this suggests a possible coexistence of SC and the DSM phase within the studied films, which can support the formation of surface Majorana modes [16,17].

Originally, the GL theory describes SC in the vicinity of T_c. However, fairly often it is applied in a much broader temperature range [34]. In our study, the application of the GL theory implies that transverse H_c values extrapolated to zero temperature can be used for the estimation of the coherence length ξ [$H_c(0) = \phi_0/(2\pi\xi^2)$, where ϕ_0 is the magnetic flux quantum]. For sample C, we obtain $\xi \approx 100$ nm (for the midpoint H_c value), which is twice as high as the film thickness. The latter suggests that the observed SC should be two dimensional, and the corresponding H_c-T_c diagram for the longitudinal field should follow Eq. (1) with $\alpha = 1, \beta = 1/2$ [35]. The temperature range, where this type of H_c-T_c correlation should be observed, depends on various parameters of the film [36]. Thus, the absence of such behavior for the studied films suggests that it may be very narrow. On the other hand, the isotropic linear character of the $H_c(T)$ dependences

may also indicate that some additional effects are relevant in our case. A more general approach [37] suggests that a linear H_c-T_c relation in the wide temperature range can be observed for systems with a strong pairing interaction. According to the phase diagram of SC in Cd_3As_2 [15,17], the type of pairing potential (even or odd parity) depends not on the integral strength of the *e*-*e* attraction, but rather on the relation between intra- and interorbital components. However, in the studies of pressure-induced SC in Cd_3As_2 [18] and Bi_2Se_3 [38,39], the linear character of the H_c-T_c diagram (alongside the saturation of the pressure dependence of T_c) was considered as a signature of nontrivial pairing (of odd parity). Similarly, in our case, the obtained H_c-T_c diagrams with a pronounced linear behavior also may indicate the presence of an odd-parity pairing potential in the studied films. However, to verify the topological nature of the observed SC, one needs to perform a set of various experiments [15], which are technologically challenging in our case and require further studies.

From the conventional point of view, the emergence of the SC phase in our case is favored due to high electron densities (the Hall concentrations for the studied films are about 8–12 $\times$ 10^{18} cm^{-3}). It implies that the Fermi level lies substantially higher than the Lifshitz transition of pristine Cd_3As_2 single crystals, meaning that the transport features of the DSM phase might be damped, although the band structure may preserve the nonzero Berry curvature [40]. Nevertheless, a substantial increase in the electron density in topological materials always precedes the emergence of the SC phase, which, however, is argued to sustain topological features [18,38,39]. Considering the fact that high-quality Cd_3As_2 single-crystalline films studied in a similar temperature range did not exhibit any SC transition [27], we assume that the SC phase in our case results from possible crystal structure distortions.

Knowing that the emergence of intrinsic SC in Cd_3As_2 is induced by pressure [18–20], we also tend to assume that the observed SC can be affected by strain existing within a film (e.g., due to the polycrystalline character). Due to the relatively small thickness of the studied films, such strain can be also related to the difference in the coefficients of thermal expansion (CTE) of the substrate and the film. At room temperature, Cd_3As_2 is characterized by a large CTE value of about $\alpha_{CdAs} \sim 11.8$–12.4×10^{-6} K^{-1}. It decreases with the temperature as it is for a normal metal [31]. Al_2O_3 has anisotropic CTE (from $\alpha_{\parallel} = 6.7 \times 10^{-6}$ K^{-1} to $\alpha_{\perp} = 5.0 \times 10^{-6}$ K^{-1}) at room temperature [41]. Si has smaller CTE at room temperatures ($\alpha_{Si} = 2.54 \times 10^{-6}$ K^{-1}) and exhibits even negative values at lower temperatures, 20–110 K [42]. Thus, as the temperature decreases, the Al_2O_3 substrate contracts less, and the Si substrate contracts even far less than the Cd_3As_2 film. As a result, the studied samples should experience the tensile strain in the temperature range under study. We did not manage to find either experimental or theoretical studies of the Cd_3As_2 phase diagram under negative pressures, making it hard to predict the effect of such strain. We observed close values of $T_c \approx 190$ mK (midpoint) for samples A (40-nm film on a Si substrate) and B (80-nm film on an Al_2O_3 substrate) with substantially different widths of the SC transition. Moreover, preliminary studies of the films deposited at the same conditions on fused quartz substrates (with $\alpha \ll \alpha_{Si}$) revealed the absence of a SC transition down to 40 mK. Thus, it is clear that the substrate strongly affects the emergent SC state in the studied films. However, to elucidate all relevant effects, an additional investigation is highly needed.

We would like to emphasize that the observation of zero resistance and the consistent character of the $I_c(T)$ and $H_c(T)$ dependences implies that the SC state is attributed to the whole sample. Due to the polycrystalline character of the studied films, the exact structure of the grain boundaries can affect the emergent SC (e.g., by changing the I_c values), which is common for many conventional SC. However, to relate the observed SC solely to the grain boundaries, one needs to assume that these boundaries have a very specific structure, which is highly unlikely to occur in a real sample.

It is important to note that the indications of surface SC in Cd_3As_2 single crystals was recently reported [43]. The apparent difference is that we observed zero resistance of the whole film, while the SC in the corresponding crystals [43] results only in a 10% drop of surface resistance. Whereas this difference may be related to various reasons, the properties of Majorana modes in our case can be different from those of a single DSM surface [17] due to Weyl orbit formation. However, as it was recently demonstrated in Josephson junction experiments [23], to reveal any particular anomalies of topological surface-mediated superconductivity, one needs to investigate corresponding phenomena within a broad range of Fermi energies, which strongly motivates further research of the studied films.

V. CONCLUSIONS

In this paper, we report an experimental observation of the emergence of superconductivity in cadmium arsenide films without any applied pressure. The superconducting nature of the transition observed in the $R(T)$ dependence is justified by differential resistance and magnetoresistivity measurements, providing the temperature dependence of the corresponding critical parameters (I_c and H_c). We argue that the observed phenomena cannot be attributed to any parasitic effects such as elemental Cd segregation or any effects related to the contact regions. The observed SC state is characterized by H_c-T_c diagrams with pronounced linear regions at intermediate temperatures for both the transverse and longitudinal magnetic fields. The deviations from an overall linear dependence at low temperatures and close to T_c can be related to the polycrystallinity of the studied films. A similar linear $H_c(T)$ dependence was considered as a signature of a nontrivial pairing potential in bulk Cd_3As_2 and Bi_2Se_3 films under pressure. Theory suggests that such a pairing potential should result in the formation of surface Majorana modes. Favored by high electron densities, the observed superconducting state can emerge due to the distortion of the film crystal structure, which arises during the deposition procedure using magnetron sputtering. We argue that this SC state can be affected by various strains arising in the films under study. We also note that similar films deposited on fused quartz substrates do not exhibit the emergence of a superconducting state down to 40 mK. Thus, it is possible to substantially affect the observed

SC state. The latter indicates that the investigated systems might be a promising platform for studies of topological superconductivity.

ACKNOWLEDGMENTS

The work was partially supported by the Russian Science Foundation, Grant No. 17-12-01345. A portion of this work was performed at the National High Magnetic Field Laboratory, which is supported by the National Science Foundation Cooperative Agreement No. DMR-1644779 and the State of Florida. A portion of the theoretical analysis, performed by V.M.P., was supported by Russian Foundation for Basic Research, Grant No. 16-29-03330. We would like to thank K. V. Mitsen and O. M. Ivanenko for fruitful discussions and H. Baek and G. Jones for technical assistance at the NHMFL.

[1] N. P. Armitage, E. J. Mele, and A. Vishwanath, Weyl and Dirac semimetals in three-dimensional solids, Rev. Mod. Phys. **90**, 015001 (2018).

[2] B. Yan and C. Felser, Topological materials: Weyl semimetals, Annu. Rev. Condens. Matter Phys. **8**, 337 (2017).

[3] S. Wang, B.-C. Lin, A.-Q. Wang, D.-P. Yu, and Z.-M. Liao, Quantum transport in Dirac and Weyl semimetals: A review, Adv. Phys.: X **2**, 518 (2017).

[4] M. Neupane, S. Y. Xu, R. Sankar, N. Alidoust, G. Bian, C. Liu, I. Belopolski, T. R. Chang, H. T. Jeng, H. Lin *et al.*, Observation of a three-dimensional topological Dirac semimetal phase in high-mobility Cd_3As_2, Nat. Commun. **5**, 3786 (2013).

[5] Z. K. Liu, J. Jiang, B. Zhou, Z. J. Wang, Y. Zhang, H. M. Weng, D. Prabhakaran, S.-K. Mo, H. Peng, P. Dudin *et al.*, A stable three-dimensional topological Dirac semimetal Cd_3As_2, Nat. Mater. **13**, 677 (2014).

[6] S. Jeon, B. B. Zhou, A. Gyenis, B. E. Feldman, I. Kimchi, A. C. Potter, Q. D. Gibson, R. J. Cava, A. Vishwanath, and A. Yazdani, Landau quantization and quasiparticle interference in the three-dimensional Dirac semimetal Cd_3As_2, Nat. Mater. **13**, 851 (2014).

[7] S. Borisenko, Q. Gibson, D. Evtushinsky, V. Zabolotnyy, B. Büchner, and R. J. Cava, Experimental Realization of a Three-Dimensional Dirac Semimetal, Phys. Rev. Lett. **113**, 027603 (2014).

[8] L. Lu, Z. Wang, D. Ye, L. Ran, L. Fu, J. D. Joannopoulos, and M. Soljačić, Experimental observation of Weyl points, Science **349**, 622 (2015).

[9] J. J. Dubowski and D. F. Williams, Pulsed laser evaporation of Cd_3As_2, Appl. Phys. Lett. **44**, 339 (1984).

[10] C. Weclewicz and L. Zdanowicz, Transport properties of thin amorphous films of cadmium arsenide, Thin Solid Films **151**, 87 (1987).

[11] A. A. El-Shazly, H. Soliman, D. Abd El-Hady, and H. E. A. El-Sayed, Transport properties of thin Cd_3As_2 polycrystalline films, Vacuum **47**, 45 (1996).

[12] B. Jarzabek, J. Weszka, and J. Cisowski, Distribution of electronic states in amorphous Cd-As thin films on the basis of optical measurements, J. Non-Cryst. Solids **333**, 206 (2004).

[13] L. A. Wray, S.-Y. Xu, Y. Xia, Y. S. Hor, D. Qian, A. V. Fedorov, H. Lin, A. Bansil, R. J. Cava, and M. Z. Hasan, Observation of topological order in a superconducting doped topological insulator, Nat. Phys. **6**, 855 (2010).

[14] Y. Ando and L. Fu, Topological crystalline insulators and topological superconductors: From concepts to materials, Annu. Rev. Condens. Matter Phys. **6**, 361 (2015).

[15] M. Sato and Y. Ando, Topological superconductors: A review, Rep. Prog. Phys. **80**, 076501 (2017).

[16] S. Kobayashi and M. Sato, Topological Superconductivity in Dirac Semimetals, Phys. Rev. Lett. **115**, 187001 (2015).

[17] T. Hashimoto, S. Kobayashi, Y. Tanaka, and M. Sato, Superconductivity in doped Dirac semimetals, Phys. Rev. B **94**, 014510 (2016).

[18] L. He, Y. Jia, S. Zhang, X. Hong, C. Jin, and S. Li, Pressure-induced superconductivity in the three-dimensional topological Dirac semimetal Cd_3As_2, npj Quantum Mater. **1**, 16014 (2016).

[19] H. Wang, H. Wang, H. Liu, H. Lu, W. Yang, S. Jia, X.-J. Liu, X. C. Xie, J. Wei, and J. Wang, Observation of superconductivity induced by a point contact on 3D Dirac semimetal Cd_3As_2 crystals, Nat. Mater. **15**, 38 (2015).

[20] L. Aggarwal, A. Gaurav, G. S. Thakur, Z. Haque, A. K. Ganguli, and G. Sheet, Unconventional superconductivity at mesoscopic point contacts on the 3D Dirac semimetal Cd_3As_2, Nat. Mater. **15**, 32 (2015).

[21] C.-Z. Li, C. Li, L.-X. Wang, S. Wang, Z.-M. Liao, A. Brinkman, and D.-P. Yu, Bulk and surface states carried supercurrent in ballistic Nb-Dirac semimetal Cd_3As_2 nanowire-Nb junctions, Phys. Rev. B **97**, 115446 (2018).

[22] W. Yu, W. Pan, D. L. Medlin, M. A. Rodriguez, S. R. Lee, Z.-q. Bao, and F. Zhang, π and 4π Josephson Effects Mediated by a Dirac Semimetal, Phys. Rev. Lett. **120**, 177704 (2018).

[23] A.-Q. Wang, C.-Z. Li, C. Li, Z.-M. Liao, A. Brinkman, and D.-P. Yu, 4π-Periodic Supercurrent from Surface States in Cd_3As_2 Nanowire-Based Josephson Junctions, Phys. Rev. Lett. **121**, 237701 (2018).

[24] M. Uchida, Y. Nakazawa, S. Nishihaya, K. Akiba, M. Kriener, Y. Kozuka, A. Miyake, Y. Taguchi, M. Tokunaga, N. Nagaosa *et al.*, Quantum Hall states observed in thin films of Dirac semimetal Cd_3As_2, Nat. Commun. **8**, 2274 (2017).

[25] T. Schumann, L. Galletti, D. A. Kealhofer, H. Kim, M. Goyal, and S. Stemmer, Observation of the Quantum Hall Effect in Confined Films of the Three-Dimensional Dirac Semimetal Cd_3As_2, Phys. Rev. Lett. **120**, 016801 (2018).

[26] C. Zhang, A. Narayan, S. Lu, J. Zhang, H. Zhang, Z. Ni, X. Yuan, Y. Liu, J.-H. Park, E. Zhang *et al.*, Evolution of Weyl orbit and quantum Hall effect in Dirac semimetal Cd_3As_2, Nat. Commun. **8**, 1272 (2017).

[27] L. Galletti, T. Schumann, O. F. Shoron, M. Goyal, D. A. Kealhofer, H. Kim, and S. Stemmer, Two-dimensional Dirac fermions in thin films of Cd_3As_2, Phys. Rev. B **97**, 115132 (2018).

[28] S. Wei, J. Lu, W. Yu, H. Zhang, and Y. Qian, Isostructural Cd_3E_2 (E = P, As) microcrystals prepared via a hydrothermal route, Cryst. Growth Des. **6**, 849 (2006).

[29] P. Cheng, C. Zhang, Y. Liu, X. Yuan, F. Song, Q. Sun, P. Zhou, D. W. Zhang, and F. Xiu, Thickness-dependent quantum

oscillations in Cd_3As_2 thin films, New J. Phys. **18**, 083003 (2016).

[30] E. Arushanov, Crystal growth and characterization of II_3V_2 compounds, Prog. Cryst. Growth Charact. Mater. **3**, 211 (1981).

[31] A. Pietraszko and K. Lukaszewicz, Thermal expansion and phase transitions of Cd_3As_2 and Zn_3As_2, Phys. Status Solidi A **18**, 723 (1973).

[32] J. R. Clement, The atomic heat and critical magnetic field of superconducting cadmium, Phys. Rev. **92**, 1578 (1953).

[33] B. B. Goodman and E. Mendoza, LXII. The critical magnetic fields of aluminium, cadmium, gallium and zinc, Philos. Mag. **42**, 594 (1951).

[34] R. Yan, G. Khalsa, S. Vishwanath, Y. Han, J. Wright, S. Rouvimov, D. S. Katzer, N. Nepal, B. P. Downey, D. A. Muller *et al.*, GaN/NbN epitaxial semiconductor/superconductor heterostructures, Nature (London) **555**, 183 (2018).

[35] K. L. Chopra, *Thin Film Phenomena* (Krieger, Malabar, FL, 1979).

[36] E. A. Shapoval, Critical fields of thin superconducting films, Zh. Eksp. Teor. Fiz. **49**, 930 (1966) [Sov. Phys. JETP **22**, 647 (1966)].

[37] E. Z. Kuchinskii, N. A. Kuleeva, and M. V. Sadovskii, Temperature dependence of the upper critical field in disordered Hubbard model with attraction, J. Exp. Theor. Phys. **125**, 1127 (2017).

[38] K. Kirshenbaum, P. S. Syers, A. P. Hope, N. P. Butch, J. R. Jeffries, S. T. Weir, J. J. Hamlin, M. B. Maple, Y. K. Vohra, and J. Paglione, Pressure-Induced Unconventional Superconducting Phase in the Topological Insulator Bi_2Se_3, Phys. Rev. Lett. **111**, 087001 (2013).

[39] P. P. Kong, J. L. Zhang, S. J. Zhang, J. Zhu, Q. Q. Liu, R. C. Yu, Z. Fang, C. Q. Jin, W. G. Yang, X. H. Yu *et al.*, Superconductivity of the topological insulator Bi_2Se_3 at high pressure, J. Phys.: Condens. Matter **25**, 362204 (2013).

[40] S. Nishihaya, M. Uchida, Y. Nakazawa, K. Akiba, M. Kriener, Y. Kozuka, A. Miyake, Y. Taguchi, M. Tokunaga, and M. Kawasaki, Negative magnetoresistance suppressed through a topological phase transition in $(Cd_{1-x}Zn_x)_3As_2$ thin films, Phys. Rev. B **97**, 245103 (2018).

[41] I. S. Grigoriev, E. Z. Meilikhov, and A. Radzig, *Handbook of Physical Quantities* (CRC Press, Boca Raton, FL, 1997).

[42] S. I. Novikova, *Thermal Expansion of Solids* (Nauka, Moscow, 1974).

[43] O. O. Shvetsov, V. D. Esin, A. V. Timonina, N. N. Kolesnikov, and E. V. Deviatov, Surface superconductivity in a three-dimensional Cd_3As_2 semimetal, arXiv:1811.02475.